Marine Chemistry 240 (2022) 104097

Contents lists available at ScienceDirect

Marine Chemistry

journal homepage: www.elsevier.com/locate/marchem

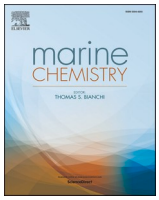

Large fluxes of continental-shelf-borne dissolved organic carbon in the East China Sea and the Yellow Sea

Heejun Han [a], Taehee Na [a], Hyung-Mi Cho [a,b], Guebuem Kim [a], Jeomshik Hwang [a,*]

[a] School of Earth and Environmental Sciences, Research Institute of Oceanography, Seoul National University, 1 Gwanak-ro, Gwanak-gu, Seoul 08826, South Korea
[b] Department of Ocean Sciences, Inha University, 100 Inha-ro, Incheon 22212, South Korea

ARTICLE INFO

Keywords:
Dissolved organic carbon
Continental shelf
Radiocarbon
East China Sea

ABSTRACT

Fluxes of dissolved organic carbon (DOC) from continental shelves to the ocean may play a critical role in marine carbon cycling and budget. However, these fluxes have been poorly constrained because complicated biogeochemical reactions of riverine, atmospheric, and marine organic carbon occur in continental shelf-waters. We used multiple tracers of DOC such as stable- and radiocarbon isotope ratios of DOC, fluorescent properties of dissolved organic matter (FDOM), and ^{228}Ra as a water age tracer to investigate the sources and fluxes of DOC in the northwest Pacific continental margin of the East China Sea and the Yellow Sea. Here, we show that there are significant additional (excess) supplies of DOC in the central Yellow Sea relative to the Changjiang (Yangtze River) source, based on these tracers. The marine δ^{13}C signature (-21.1 ± 1.1‰) and the radiocarbon age (2000 $\pm$ 400 yr) of DOC suggest that the additional DOC (Δ^{14}DOC = -44‰) is supplied from a combination of newly produced DOC and the degradation of particulate as well as sedimentary organic matter. The flux of this additional DOC produced in the continental shelf of the East China Sea to the open ocean is estimated to be ~1.9 $\pm$ 0.8 Tg C yr^{-1}, which is comparable to that from the Changjiang discharge. Our study implies that the fluxes of continental shelf-borne DOC may be important globally and should be considered in estimating global DOC budgets in the marine environment.

1. Introduction

Dissolved organic carbon (DOC) comprises the largest pools (660 Pg C) of reduced carbon in the ocean (Hopkinson and Vallino, 2005; Follett et al., 2014). DOC is mainly produced by primary production and other processes including grazing, dissolution of sinking particles, and microbial activity in the ocean (Carlson and Hansell, 2015). In the coastal ocean, terrigenous DOC transported via the atmosphere, rivers, and groundwater contribute significantly to the carbon budget (Kuhlbusch, 1998; Masiello and Druffel, 1998; Raymond and Bauer, 2001a; Raymond and Bauer, 2001b; Guo and Macdonald, 2006; Yan and Kim, 2012; Huang et al., 2012; Kim et al., 2013; Lee and Kim, 2018). The global annual flux of DOC to the oceans through rivers is 0.17–0.36 Pg C yr^{-1} (Maybeck, 1982; Dai et al., 2012; Bauer et al., 2013). The global DOC flux via groundwater is estimated to supply an additional 0.12 Pg C yr^{-1} to the oceans (Chen et al., 2018). The atmospheric deposition of DOC (wet deposition) to the ocean surface is estimated to be 0.09–0.25 Pg C yr^{-1} (Willey et al., 2000; Kanakidou et al., 2012).

Continental shelves are a dynamic zone where terrestrial and oceanic DOC are introduced and processed (Hedges and Kiel, 1995). Because of high primary production on the shelves in general, in situ production of DOC and DOC flux from the degradation of particulate organic carbon (POC) in the water column and bottom sediments should be a major part of the carbon budget on the shelves in addition to the external source inputs. Furthermore, DOC produced in the continental shelves has the potential to be exported to the open ocean (Burdige et al., 1999; Bauer et al., 2013). However, the potential role of the continental shelves as an important DOC source in the ocean carbon budget is not well understood.

In this study, we attempted to characterize the sources and fluxes of DOC in the East China Sea (ECS) and the Yellow Sea. The ECS continental shelf is one of the largest continental shelves in the world (Wang et al., 2000). In this region, the Changjiang (Yangtze River) reportedly discharges ~1.6 Tg C yr^{-1} of DOC and ~ 1.5 Tg C yr^{-1} of POC to the ECS (Wang et al., 2012; Shi et al., 2016). In the northern part of this region, the Yellow River discharges ~0.03 Tg C yr^{-1} of DOC and ~ 0.39 Tg C yr^{-1} of POC to the Yellow Sea (Wang et al., 2012; Shi et al., 2016). The Yellow Sea is a productive semi-enclosed marginal sea in the northwest

* Corresponding author.
E-mail address: jeomshik@snu.ac.kr (J. Hwang).

https://doi.org/10.1016/j.marchem.2022.104097
Received 3 September 2019; Received in revised form 20 December 2021; Accepted 14 February 2022
Available online 17 February 2022

Pacific, where the annual net primary production is estimated as ~145 g C m^{-2} yr^{-1} based on satellite observation (Gong et al., 2003). In addition, carbon export off the shelf to the open ocean, termed the "continental shelf pump," has been investigated in this productive region (Tsunogai et al., 1999).

In order to study DOC cycling with a special focus on its input from various sources and export from the shelf, we used multiple tracers including naturally occurring ^{228}Ra, ^{13}C and ^{14}C contents in DOC, and the characteristics of fluorescent dissolved organic matter (FDOM) in the water column. ^{228}Ra isotope (half-life: 5.75 yr) is an effective tool in this region for differentiating water masses and their age determination because it is highly soluble and becomes enriched by benthic and riverine inputs (Nozaki et al., 1991; Kim et al., 2005). The benthic inputs of ^{228}Ra include diffusion from sediments, where particle-reactive ^{232}Th (half-life: 1.4×10^{10} yr) has accumulated, and from submarine groundwater discharge in this region (Kim et al., 2005; Lee et al., 2014; Kim et al., 2018). The ages of water masses can be determined using the rapid decay of ^{228}Ra relative to ^{226}Ra (half-life: 1600 yr) (Nozaki et al., 1990). Stable carbon isotope ratio (δ^{13}C) measurement allows one to differentiate marine (−18‰ to −22‰) versus terrestrial (−26‰ to −32‰) sources of organic matter (Gearing, 1998; Raymond and Bauer, 2001b; Wang et al., 2012; Lee and Kim, 2018). Radiocarbon (^{14}C) measurement of DOC is useful for determining carbon cycling including sources, ages, and its residence time (Druffel and Bauer, 2000; Walker et al., 2014). The average ^{14}C age of oceanic DOC is 4000–6500 years in the deep ocean (>2000 m) and 1000–4000 years in surface waters (Williams and Druffel, 1987; Druffel, 1992; Druffel and Bauer, 2000). Terrestrial DOC-Δ^{14}C values are usually distinctly different from marine DOC (Raymond and Bauer, 2001a; Raymond and Bauer, 2001b). Fresh DOC exported via rivers or produced in situ is generally younger and enriched with ^{14}C, while the deep marine DOC is relatively old and ^{14}C-depleted although the individual compounds can have a wide age spectrum (Hedges et al., 1986; Williams and Druffel, 1987; Druffel, 1992; Druffel and Bauer, 2000; Raymond and Bauer, 2001b). The light-absorbing fraction of reduced organic matter is termed colored dissolved organic matter (CDOM) (Coble, 2007). A part of CDOM that fluoresces over a wide range of wavelengths after absorbing energy is called FDOM (Coble, 2007). The humic-like components of FDOM ($FDOM_H$) are useful for tracing DOC due to their conservative nature in the ocean (Kowalczuk et al., 2003; Kowalczuk et al., 2010; Fichot and Benner, 2012; Kim and Kim, 2015; Painter et al., 2018). In particular, $FDOM_H$ component, together with ^{228}Ra tracers, has been used to identify the inputs of $FDOM_H$ from the marine sediment in this region (Kim et al., 2018).

2. Materials and methods

2.1. Study region and sampling

The study region is located in the continental shelf of the northern ECS and the Yellow Sea (Fig. 1). In this region, the Yellow Sea water (YSW), the Kuroshio Current water (KCW), and the Changjiang diluted water (CDW) are present with varying seasonal contributions (Kim et al., 2018; Wang et al., 2000) (Fig. 1). Although the YSW originates from both the KCW and the CDW, its biogeochemical characteristics are significantly altered during its residence time of about five years in the Yellow Sea (Nozaki et al., 1991; Kim et al., 2005). In this region, the Changjiang plays a dominant role in supplying ~80% of freshwater and delivering terrestrial carbon to the adjacent seas (Ichikawa and Beardsley, 2002; Wang et al., 2012; Bauer et al., 2013). In general, the Changjiang flows northeastward upon entering the Yellow Sea in summer, while it flows southward along the Chinese coast in winter (Ichikawa and Beardsley, 2002; Chen, 2009; Lie and Cho, 2016). Thus, in the study region, the influence of the CDW was observed only in summer, and was not observed in winter and spring seasons (Ichikawa and Beardsley, 2002; Chen, 2009; Kim et al., 2018; Lie and Cho, 2016) (Fig. 1). In this study, the KCW includes both the Kuroshio surface water (KSW) and the Kuroshio tropical water (KTW). The current system in the study region has been well documented in several previous studies (Ichikawa and Beardsley, 2002; Chen, 2009; Lie and Cho, 2016; Fig. 1).

Sampling was conducted four times from August to September in 2012 (summer): 11–13 August aboard the R/V *Tamgu 3* of the National Fisheries Research and Development Institute (NFRDI), 13–14 August aboard the *Badaro* of the Korea Coast Guard, 21–22 August and 1–4 September aboard R/V *Tamgu 8* of the NFRDI. Further sampling was conducted in February 2017 (winter) and April 2018 (spring) aboard the R/V *Onnuri* of the Korea Institute of Ocean Science and Technology (KIOST). Seawater samples were collected using 10 L Niskin bottles mounted on a rosette system equipped with a conductivity temperature and depth device (CTD). In 2012, sampling was conducted for the surface water (1–2 m) only at most of the stations except for four stations where water column samples were collected. In 2017 and 2018,

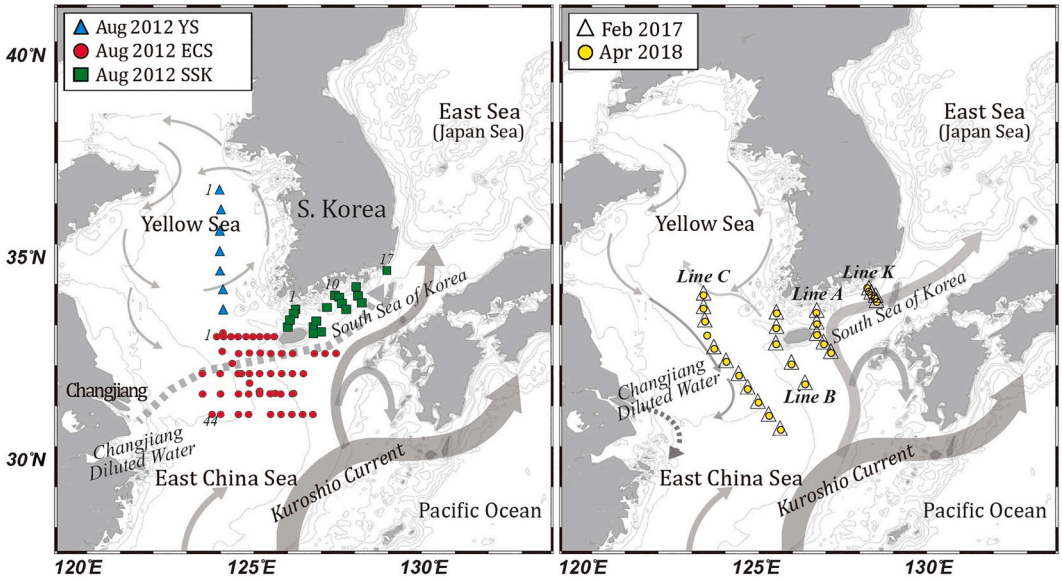

Fig. 1. Maps of sampling stations, bottom topography, and schematic patterns of surface currents on the continental shelf of the East China Sea and the Yellow Sea during the sampling periods. (For interpretation of the references to colour in this figure legend, the reader is referred to the web version of this article.)

sampling was conducted for the water column at all stations.

Seawater samples were filtered through pre-combusted (450 °C for 5 h) GF/F filters (pore size = 0.7 μm; Whatman). Samples for DOC concentration and stable carbon isotope analysis were acidified with 6 N HCl to suppress any bacterial activities and stored in pre-combusted glass ampoules. Samples for DOC-$\Delta^{14}C$ analysis were stored in pre-combusted amber Boston round glass bottles at −20 °C. Samples for FDOM analysis were stored in pre-combusted amber glass vials in a refrigerator at 4 °C.

2.2. Chemical analyses

For the determination of DOC concentrations, samples were analyzed by a high-temperature catalytic oxidation (HTCO) method using a total organic carbon (TOC) analyzer (TOC-V_{CPH}, Shimadzu, Japan) (Kim and Kim, 2010). Analysis was also conducted on a certified reference material of deep seawater (~43 μM DOC; University of Miami) (Hansell, 2005). The precision of measurement was ±2.0 μM based on multiple analyses.

FDOM was measured using a spectrofluorometer (Aqualog, Horiba). Excitation-emission matrix spectroscopy (EEMs) analysis was conducted by detecting emission and excitation wavelengths of 250–600 nm and 250–500 nm, respectively, with 2 nm scanning intervals. The parallel factor analysis (PARAFAC) model was applied to characterize the major fluorescent components (Bro, 1997; Stedmon and Bro, 2008). The blank subtraction, Raman and Rayleigh scattering signals, and inner-filter effect were corrected using the Solo software (Eigenvector, 108 Inc.). The fluorescence intensities were normalized with Raman peak area of pure water and presented as Raman unit (R.U.) (Lawaetz and Stedmon, 2009). The PARAFAC model characterized three components: terrestrial humic-like (Ex/Em = 284/427 nm; C peak), marine humic-like (Ex/Em = 276/340 nm; M peak), and protein-like (tryptophan-like) fluorescent components (Ex/Em = 264/313 nm; T peak). Details of FDOM analysis are given in Kim et al. (2018). In this study, only terrestrial humic-like component ($FDOM_H$) data were used.

Stable carbon ($\delta^{13}C$) and natural radiocarbon ($\Delta^{14}C$) abundances were measured for DOC samples collected from stations on lines C and A in February 2017 only. The $\delta^{13}C$ values of DOC (DOC-$\delta^{13}C$) were measured using isotope ratio mass spectrometer (IRMS) (Isoprime, Elementar) aligned with a TOC analyzer (TOC–IRMS) (Lee and Kim, 2018). CO_2 gas from the non-dispersive infrared sensor (NDIR) was introduced to IRMS via an interface (Panetta et al., 2008; Troyer et al., 2010). The isotopic composition DOC–$\delta^{13}C$ is reported on Vienna Pee Dee Belemnite (VPDB) scale (Troyer et al., 2010). Analysis was conducted on certified IAEA-CH6 sucrose ($\delta^{13}C = -10.45 \pm 0.03$‰; International Atomic Energy Agency), reference material of deep seawater (DSR; $\delta^{13}C = -21.5 \pm 0.1$‰; University of Miami), and Suwannee River Fulvic Acid (SRFA) ($\delta^{13}C = -27.6 \pm 0.12$‰; International Humic Substances Society) to evaluate the recovery and accuracy of the measurements (Hansell, 2005; Lang et al., 2007; Panetta et al., 2008; Troyer et al., 2010). For DOC-$\Delta^{14}C$ measurements, samples were acidified to ~pH 2 with 85% phosphoric acid, purged with ultra-high purity nitrogen gas to remove dissolved inorganic carbon, and oxidized by UV irradiation (Beaupre et al., 2007). The resultant CO_2 gas was analyzed for radiocarbon isotope ratio at the National Ocean Sciences Accelerator Mass Spectrometry Facility (NOSAMS) at the Woods Hole Oceanographic Institution.

For ^{228}Ra measurement, seawater samples (100*L*) were collected in polypropylene cubitainers. Seawater was passed through a column of acrylic fiber impregnated with MnO_2 (Mn-fiber) at <1 L min^{-1} by gravity on board (Moore, 1976). The Mn-fiber was rinsed gently with Ra-free deionized water to wash out any salts or particles, then ashed at 820 °C for 16 h in a land-based laboratory. The ashed Mn-fiber was transferred to hermetically sealed vials and analyzed for ^{228}Ra using a high-purity Germanium well-type detector (CANBERRA Industries Inc.). ^{228}Ra activities were determined by counting the gamma peaks at 911 keV from its daughter ^{228}Ac (Kim et al., 2003). The geometry effect on the detection efficiency was corrected and applied to the final activity calculations. We also used the ^{228}Ra data in August 2012 from Lee et al. (2014) and in February 2017 from Kim et al. (2018).

3. Results and discussion

3.1. Water masses and distributions of DOC, $FDOM_H$, and ^{228}Ra

In this study, five major water masses were distinguished based on the temperature versus salinity (T-S) distributions: the CDW, the KSW, the KTW, the Yellow Sea bottom water (YSBW), and the YSW (Hur et al., 1999; Chen, 2009; Kim et al., 2018) (Fig. 2). In summer, the water masses mainly consisted of the CDW and the KCW (Fig. 2). In winter and spring, temperature and salinity varied depending on the relative contributions of the YSW, YSBW, and KTW (Fig. 2). The CDW (salinity: <33; temperature: 27–29 °C), which is characterized by high temperature and low salinity, was mainly observed in the central region of the Yellow Sea only in summer 2012 (Lee et al., 2014) (Fig. 2). In general, the KTW flows underneath the KSW (Chen, 2009).

The DOC concentrations ranged from 63 to 134 μM (average = 94 ± 14 μM; average means the arithmetic mean throughout the paper) in summer, from 51 to 108 μM (average = 62 ± 10 μM) in winter, and from 55 to 143 μM (average = 69 ± 11 μM) in spring. The higher DOC values were mainly observed for the CDW in low-salinity waters (<33) in summer 2012, while the higher DOC value was observed in high-salinity waters (>33) in April 2018 (Fig. 3). Spatially, the DOC concentrations in the surface water were highest near the central Yellow Sea and gradually decreased toward the ECS and the southern sea of Korea in all sampling periods (Fig. 3). Overall, the DOC concentrations were higher in the YSW than in the KTW in both winter and spring (Fig. 2).

The concentrations of $FDOM_H$ ranged from 0.5 to 2.7 RU (average = 1.3 ± 0.4 RU) in summer, from 0.2 to 2.3 RU (average = 0.8 ± 0.4 RU) in winter, and from 0.1 to 1.2 (average = 0.5 ± 0.3 RU) in spring (Figs. 2, 4b). The concentrations of $FDOM_H$ in the surface water showed a similar spatial distribution with that of DOC trends in general (Fig. 3, Supplementary Fig. 1).

^{228}Ra activity concentrations were in the range of 10–58 dpm 100 L^{-1} (average = 29 ± 10 dpm 100 L^{-1}) in summer, 7–58 dpm 100 L^{-1} (average = 29 ± 17 dpm 100 L^{-1}) in winter, and 4–58 dpm 100 L^{-1} (average = 23 ± 17 dpm 100 L^{-1}) in spring (Fig. 2). The highest ^{228}Ra activity concentration was found in the YSBW, while the lowest concentration was found in the KTW (Fig. 2f, i). However, activities higher than 40 dpm 100 L^{-1} were also observed in the CDW in summer 2012 (Fig. 2c).

3.2. Seasonal variations in the source of additional DOC in the YSW

For all sampling periods, the DOC and $FDOM_H$ concentrations showed significant correlations with salinity (Fig. 4a, b). Despite the different salinity ranges, DOC and $FDOM_H$ from three different seasons showed a common relationship against salinity (Fig. 4a, b). In summer, DOC and $FDOM_H$ appear to be mainly influenced by the CDW due to their conservative mixing against salinity (Fig. 4a, b). However, the extrapolated DOC value (~420 μM) at zero salinity was approximately twice higher than that of previously reported values in the Changjiang mouth (~160–230 μM) at zero salinity (Shi et al., 2016; Liu and Gao, 2019) (Fig. 4a). This indicates that there is an additional input of DOC. In this region, Kim et al. (2020) suggested the existence of a DOC "pulse" in the salinity range of 24–35 due to the microbial metabolism in the estuarine mixing zone (Fig. 4a). The existence of this process is also supported by the high primary production rate in the inner shelf of the ECS during summer (Gong et al., 2003).

However, in winter and spring, deviation toward higher values off the mixing line was observed for stations in the Yellow Sea (Fig. 4a). Significant deviations toward higher values off the two end-member

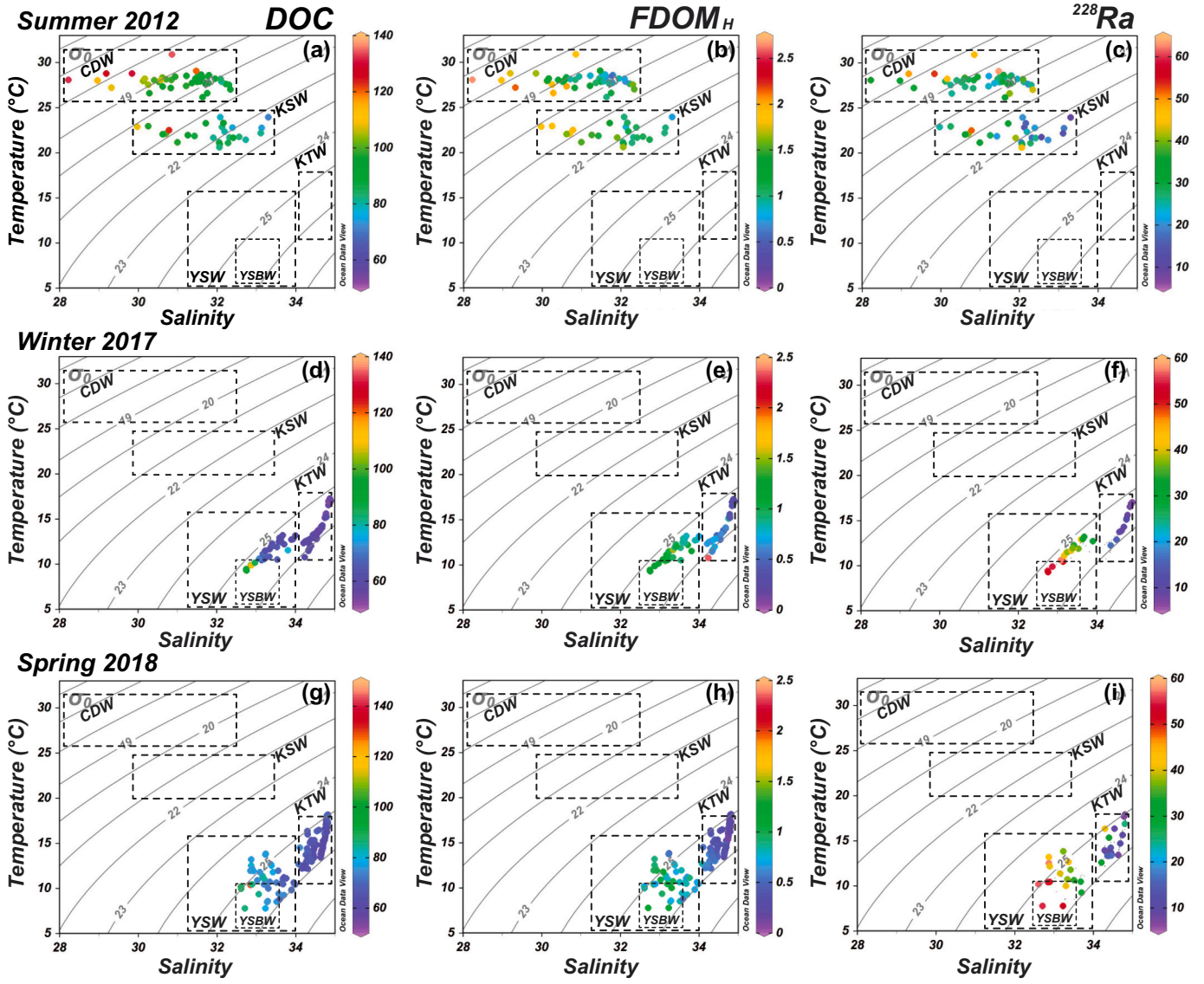

Fig. 2. T-S diagrams of DOC concentrations (a, d, g), $FDOM_H$ (b, e, h), and ^{228}Ra activities (c, f, i) in summer 2012, winter 2017, and spring 2018. Each dashed box indicates different water masses in this region: Changjiang diluted water (CDW), Kuroshio surface water (KSW), Kuroshio tropical water (KTW), Yellow Sea water (YSW), and Yellow Sea bottom water (YSBW). Dashed grey lines represent the sigma-t (σ_t). The T-S diagrams were created using Ocean Data View software version 4. 7. 6. (For interpretation of the references to colour in this figure legend, the reader is referred to the web version of this article.)

mixing line at salinity range 32.5–33.5 indicate a pronounced addition of DOC in the YSW (Fig. 4a). Also, these deviations in winter and spring were not related to the direct influence of the CDW (Fig. 2). To further reveal the causes of the deviations toward high values and the characteristics of DOC and $FDOM_H$ production in the YSW, especially in winter and spring, these DOM components were plotted against ^{228}Ra activity concentration, a tracer of the water residence time of the YSW (Nozaki et al., 1989). In the Yellow Sea, ^{228}Ra activity concentrations increase toward the central area up to 73 dpm 100 L^{-1}, which is about 9–66 times higher than that in the KCW, due to benthic inputs (Nozaki et al., 1991; Kim et al., 2005; Kawakami and Kusakabe, 2008; Lee et al., 2014). Although rivers are commonly known as the major source of ^{228}Ra in the oceans, the riverine flux is <10% of the benthic inputs in the Yellow Sea (Lee et al., 2014; Kim et al., 2015; Kim et al., 2018). Thus, ^{228}Ra can be used as an indicator of the age of YSW. Both DOC and $FDOM_H$ were significantly correlated with the ^{228}Ra activity concentrations, implying their association with the water ages in this region (Fig. 4c, d). Based on a significant correlation between ^{228}Ra and $FDOM_H$ (Fig. 4d), Kim et al. (2018) suggested that $FDOM_H$ from the bottom sediment pore water is continuously produced and accumulates in the bottom water layer. It was further suggested that the flux of $FDOM_H$ produced from organic matter degradation in the organic-rich shelf sediments was equivalent to 30–40% of the riverine source in the ECS continental shelf (Kim et al., 2018). Here, similar correlations of both DOC and $FDOM_H$ with ^{228}Ra imply that the DOC could also be produced by the re-mineralization of particulate organic matter (POM) either in the water column or surface sediments in a similar mechanism with $FDOM_H$ as suggested by Chen et al. (1993) (Fig. 4c, d).

Since the distributions of DOC and $FDOM_H$ were highly associated with the water masses and ages as explained above (Fig. 4c, d), the mixing ratios among the major water masses (the CDW, KCW, and YSW) in this region were examined from the ^{228}Ra–salinity relationship (Fig. 5). The end-member values of ^{228}Ra and salinity (marked with star symbol in Fig. 5) were assigned as 7.6, 36.3, and 78.7 dpm 100 L^{-1} and 34.7, 27.8, and 31.5 for the KCW, CDW, and YSW, respectively, based on this study and from the literature data (Nozaki et al., 1991; Gu et al., 2012; Lee et al., 2014). In summer, most data plotted along the mixing line between the CDW and the KCW with additional inputs from the

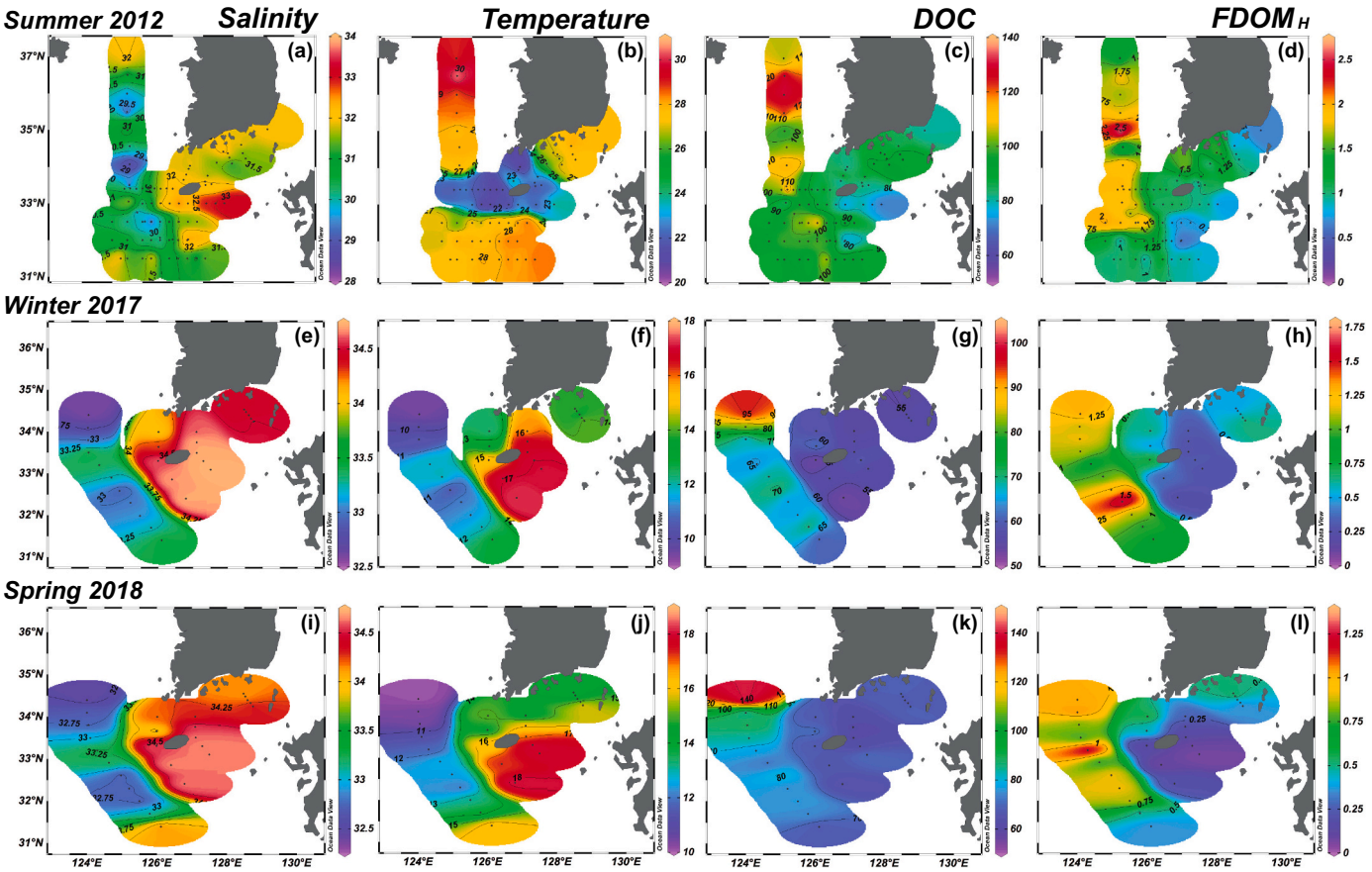

Fig. 3. Contour figures of (a, e, i) salinity, (b, f, j) temperature, (c, g, k) DOC, and (d, h, l) $FDOM_H$ in the surface water of the ECS continental shelf in summer 2012, winter 2017, and spring 2018. The contour plots were created using Ocean Data View software version 4. 7. 6.

YSW (red circles in Fig. 5). However, winter and spring data were clearly on the mixing line between the YSW and the KCW only (Fig. 5). Based on this diagram (Fig. 5), the proportion of the YSW in the mixture of the YSW and the KCW, *f*, was calculated for the winter and spring data. As the two end-member mixing model was applied for these seasons, the *f* value would be 1 if the water were composed of the YSW only. The relative proportions of the YSW, *f* values, showed a positive correlation with DOC (Fig. 6a). In Fig. 6a, an outlier (DOC, 143 μM) was excluded based on a 95% confidence interval test (Fig. 6c). Based on the relationship between DOC and *f* value, the end-member value in the YSW, when the DOC concentration was extrapolated to $f = 1$, was estimated to be 101 ± 12 μM (the uncertainty was estimated with 95% confidence interval of the linear regression; Fig. 6a). This end-member value is lower than the highest DOC values observed in the Yellow Sea (up to 140 μM) and should be regarded as DOC enrichment during the water residence time of the YSW, excluding the seasonal fluctuation. However, this end-member value is higher than the KCW DOC value (55 μM) by ~45 ± 12 μM (Fig. 6a).

The *f* value based on the two end-member mixing model between the KCW and the YSW also exhibited positive correlations with $FDOM_H$ and DOC-Δ^{14}C (Fig. 6b, c). In contrast, DOC-δ^{13}C values were constant (average = −21.1 ± 1.1‰), regardless of *f* values (Fig. 6d). The average DOC-δ^{13} value of the Changjiang, −30.3 ± 1.2‰ (Wang et al., 2012), was considerably lower than the observed DOC-δ^{13} values of −18.8‰ to −22.8‰ (average = −21.1 ± 1.1‰; Fig. 6d), indicating that there was only a small contribution of riverine DOC to the YSW DOC pool at most. This finding is consistent with the little input of the CDW to the Yellow Sea during winter and spring. As the average δ^{13}C value in surface sediments of the central Yellow Sea is −22.2 ± 0.3‰ (Bao et al., 2016), the measured DOC-δ^{13}C values could be from either water column production or from surface sediments.

The DOC-Δ^{14}C values were − 271 ± 18‰ (2500 ± 200 yr; $n = 9$) along with Line A (Fig. 1), where the KCW was dominantly observed. The DOC-Δ^{14}C values were slightly higher, −222 ± 38‰ (2000 ± 400 yr; $n = 14$), along with Line C (Fig. 1), where the YSW was observed (Fig. 6c). The end-member value of DOC-Δ^{14}C in the YSW (when $f = 1$) was estimated as −170 ± 50‰ by extrapolation (Fig. 6c), which is higher than that of the end-member DOC-Δ^{14}C value (−271 ± 18‰) in the KCW (when $f = 0$). Then, the Δ^{14}C value of the DOC added to the DOC pool in the YSW was estimated to be approximately −44‰, based on a simple mass balance calculation: $(\Delta^{14}DOC_{KCW} \times DOC_{KCW}) + (\Delta^{14}DOC_{excess} \times DOC_{excess}) = (\Delta^{14}DOC_{YSW} \times DOC_{YSW})$. This value appears to be due to the mixture of newly produced fresh DOC (Δ^{14}C = 0‰, the average of three results of dissolved inorganic carbon in the surface water of the ECS, collected in August 2020 by Sunmin Oh, unpublished data) and aged POM from the surface sediment (Δ^{14}C = −174‰ to −280‰) in this region (Bao et al., 2016). In this study, the additional DOC may consist mainly of semi-labile and refractory fractions of DOC since the DOC (^{228}Ra normalized) increased linearly with the water age (Fig. 6a). The labile fraction of DOC may vary markedly and decompose rapidly through microbial or photochemical degradation (< 1 yr; Hung et al., 2003), and thus it is not included in the DOC accumulation with the water age (~ 5 yr).

3.3. Estimation of the shelf-borne DOC flux

The DOC concentrations of the Yellow Sea, as estimated from ^{228}Ra, are significantly higher than that of the ECS. Thus, DOC should be exported out of the Yellow Sea via water exchange. We attempted to estimate the flux of excess DOC produced in the YSW into the ECS using

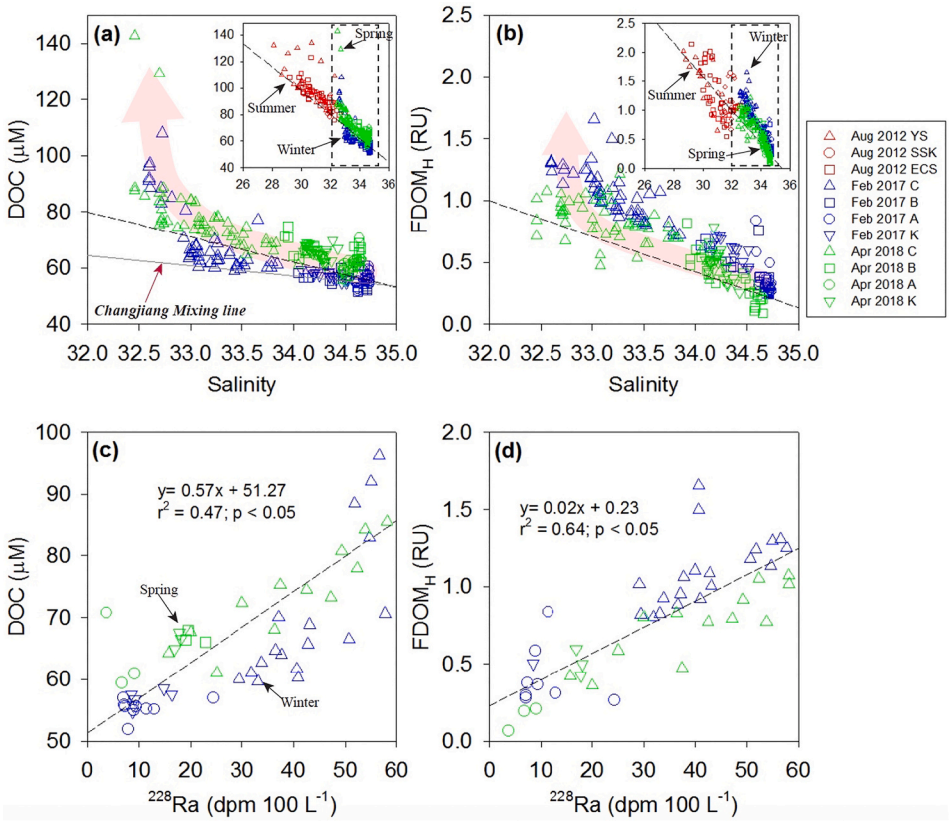

Fig. 4. Correlations between the concentration of (a) DOC and (b) $FDOM_H$ against the salinity and the concentration of (c) DOC and (d) $FDOM_H$ against the activities of ^{228}Ra in the continental shelf waters during the sampling periods. $FDOM_H$ and ^{228}Ra data in 2012 and 2017 are from Kim et al. (2018) and Lee et al. (2014). Dashed lines represent the regression lines, while the solid line represents the end-member mixing line.

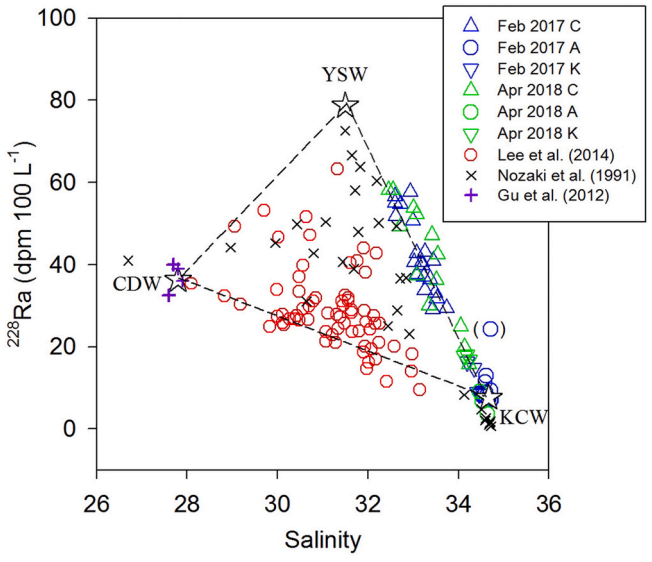

Fig. 5. A mixing diagram between the activities of ^{228}Ra and salinity. YSW, Yellow Sea water; CDW, Changjiang diluted water; KCW, Kuroshio Current water. (For interpretation of the references to colour in this figure legend, the reader is referred to the web version of this article.)

the following equation:

$$\boldsymbol{Flux} = \frac{(\boldsymbol{DOC_{YSW}} - \boldsymbol{DOC_{KCW}}) \times \boldsymbol{V_{YSW}}}{\boldsymbol{\tau_{YSW}}}$$

where DOC_{YSW} and DOC_{KCW} are the end-member values of DOC in the YSW and the KCW, respectively. The end-member value of DOC_{YSW} was obtained by extrapolation of the relationship between f and DOC described above (i.e., 101 ± 11 μM), whereas the DOC_{KCW} (55 ± 11 μM) is the average value of the observed DOC values at line A (Station A1 to A5 in Fig. 1), which is located on the main path of the Tsushima Warm Current, a branch of the Kuroshio. Here, the end-member value of DOC_{YSW} excluded significantly high DOC values (i.e., 129–143 μM) as mentioned earlier. In this estimation, the end-member values of DOC have ±20% of uncertainty each based on the 95% confidence interval (Fig. 6a). V_{YSW} is the total water volume (unit: km^3) of the YSW volume (1.7×10^{13} m^3) with a conservative uncertainty of ±20% (Yunshan et al., 1988; Li et al., 2015), and τ_{YSW} is the water residence time of the YSW, ~5 ± 1 years (Nozaki et al., 1991; Kim et al., 2005). The annual flux of the shelf-borne DOC from the Yellow Sea to the ECS was estimated to be ~1.9 Tg C yr^{-1}, with the propagated uncertainty of ~44% (±0.8 Tg C yr^{-1}). This flux of shelf-borne DOC is at least comparable to the DOC flux from the Changjiang discharge (~1.6 Tg C yr^{-1}, Wang et al., 2012; Shi et al., 2016). Despite the large uncertainty, ~44%, our estimation underlines the importance of continental-shelf-borne sources of DOC in the ocean.

4. Implications and conclusions

Studies of DOC fluxes from continental margins of regional and global scales have revealed the important role of shelf-borne DOC in carbon budget and cycle. The DOC fluxes vary widely depending on the location. The Hebrides Shelf in the North Atlantic Ocean exports DOC flux of 0.13 Tg C daily to the open ocean in winter (Painter et al., 2016). In Antarctica, the shelf water contributes approximately 4 to 8 Tg C yr^{-1} of DOC to the deep waters of the Southern Ocean (Fang et al., 2018). Recently, the estimated DOC flux was ~0.7–1.0 Pg C yr^{-1} in the Arctic

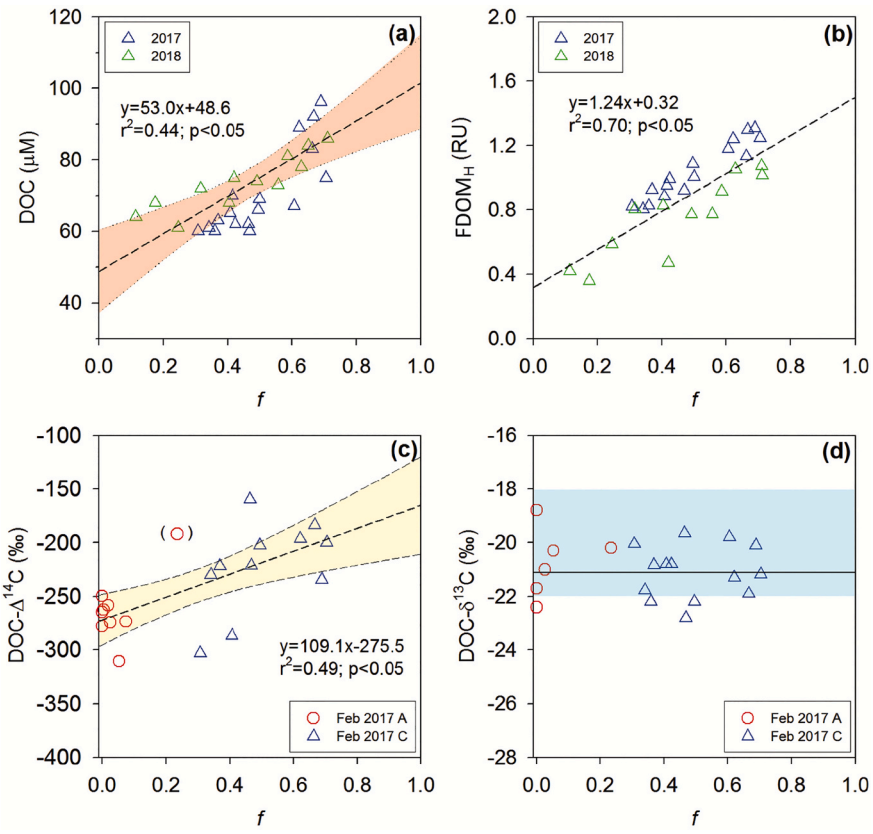

Fig. 6. Correlations between the mixing fraction, f, (f = 0 for KCW and f = 1 for YSW) against (a) DOC, (b) $FDOM_H$, (c) DOC-$\Delta^{14}C$, and (d) DOC-$\delta^{13}C$ values. Dashed lines represent end-member mixing lines. The shaded areas in parts (a) and (c) represent the 95% confidence interval of the linear regression and the blue shaded area in part (d) represents the marine signature range of $\delta^{13}C$ values. (For interpretation of the references to colour in this figure legend, the reader is referred to the web version of this article.)

shelf region, indicating that the Arctic shelf could be a major source of organic matter to the Arctic Ocean (Chen et al., 2021). The cross-shelf DOC flux from the middle Atlantic Bight to the open ocean was estimated to be 29 Tg C yr^{-1} (Mannino et al., 2016). The global export of DOC from continental shelves to the open ocean was reported as 150–350 Tg C yr^{-1}, which is comparable to the global riverine DOC flux (200 Tg C yr^{-1}) to the ocean (Maybeck, 1982; Bauer et al., 2013). Furthermore, the global DOC fluxes from productive coastal settings, including salt marsh, mangrove, intertidal, and continental shelf, were found to be even more significant (106–416 Tg C yr^{-1}) (Maher and Eyre, 2010).

In this study, we measured the shelf-borne production of DOC for the first time, based on the excess DOC inventory in seawater on a basin-scale by tracing its source using dual carbon isotope (^{13}C and ^{14}C), ^{228}Ra, and FDOM. We show that there are notable additional supplies of DOC on the continental shelf of the ECS. The source of this additional DOC was found to be a combination of newly produced DOC and degradation of fresh POM and sedimentary organic matter. The estimated export from the continental shelf of the ECS to the open ocean per year is ~1.9 ± 0.8 Tg C (albeit with a large uncertainty); thus, the continental shelf-borne DOC flux should be considered in global marine carbon budgets and cycles, and further studies are necessary for other important shelves. In addition, our multi-pronged approach will be useful in estimating DOC exports from similar geographic environments such as semi-enclosed bays.

Declaration of Competing Interest

None.

Acknowledgments

This research was supported by the project titled "Deep Water Circulation and Material Cycling in the East Sea (20160400)" funded by the Ministry of Oceans and Fisheries, Korea, and the National Research Foundation (NRF) funded by the Korean Government (NRF-2018R1A2B3001147). H. Han was partly supported by Basic Science Research Program through the National Research Foundation of Korea (NRF) funded by the Ministry of Education (2021R1A6A3A01086864). We thank laboratory members for their assistance during the sampling campaigns.

Appendix A. Supplementary data

Supplementary data to this article can be found online at https://doi.org/10.1016/j.marchem.2022.104097.

References

Bao, R., McIntyre, C., Zhao, M., Zhu, C., Kao, S.-J., Eglinton, T.I., 2016. Widespread dispersal and aging of organic carbon in shallow marginal seas. Geology 44 (10), 791–794.
Bauer, J.E., Cai, W.-J., Raymond, P.A., Bianchi, T.S., Hopkinson, C.S., Regnier, P.A.G., 2013. The changing carbon cycle of the coastal ocean. Nature 504, 61–70.
Beaupre, S.R., Druffel, E.R.M., Griffin, S., 2007. A low blank photochemical extraction system for concentration and isotopic analyses of marine dissolved organic carbon. Limnol. Oceanogr. Methods 5 (6), 174–184.
Bro, R., 1997. PARAFAC. Tutorial and applications. Chemom. Intell. Lab. Syst. 38 (2), 149–171.
Burdige, D.J., Berelson, W.M., Coale, K.H., McManus, J., Johnson, K.S., 1999. Fluxes of dissolved organic carbon from California continental margin sediments. Geochim. Cosmochim. Acta 63 (10), 1507–1515.
Carlson, C.A., Hansell, D.A., 2015. DOM sources, sinks, reactivity, and budgets. In: Hansell, D.A., Carlson, C.A. (Eds.), Biogoechemistry of Marine Dissolved Organic Matter, 2nd ed. Academic Press, Boston, pp. 65–126.
Chen, C.-T.A., 2009. Chemical and physical fronts in the Bohai, yellow and East China seas. J. Mar. Syst. 78 (3), 394–410.
Chen, R.F., Bada, J.L., Suzuki, Y., 1993. The relationship between dissolved organic carbon (DOC) and fluorescence in anoxic marine porewaters: implications for estimating benthic DOC fluxes. Geochim. Cosmochim. Acta 57, 2149–2153.

Chen, X., Zhang, F., Lao, Y., Wang, X., Du, J., Santos, I.R., 2018. Submarine groundwater discharge-derived carbon fluxes in mangroves: an important component of blue carbon budgets? J. Geophys. Res. Oceans 123, 6962–6979.
Chen, M., Kim, J.-H., Lee, Y.K., Lee, D.-H., Jin, Y.K., Hur, J., 2021. Subsea permafrost as a potential major source of dissolved organic matter to the East Siberian Arctic shelf. Sci. Total Environ. 777, 146100.
Coble, P.G., 2007. Marine optical biogeochemistry: the chemistry of ocean color. Chem. Rev. 107, 402–418.
Dai, M., Yin, Z., Meng, F., Liu, Q., Cai, W.-J., 2012. Spatial distribution of riverine DOC inputs to the ocean: an updated global synthesis. Curr. Opin. Environ. Sustain. 4 (2), 170–178.
Druffel, E.R.M., 1992. Cycling of dissolved and particulate organic matter in the open ocean. J. Geophys. Res. 97 (C10), 639–659.
Druffel, E.R.M., Bauer, J.E., 2000. Radiocarbon distributions in Southern Ocean dissolved and particulate organic matter. Geophys. Res. Lett. 27 (10), 1495–1498.
Fang, Z., Yang, W., Chen, M., Stubbins, A., Ma, H., Jia, R., Li, Q., Chen, Q., 2018. Transport of dissolved black carbon from the Prydz Bay shelf, Antarctica to the deep Southern Ocean. Limnol. Oceanogr. 63, 2179–2190.
Fichot, C.G., Benner, R., 2012. The spectral coefficient of chromophoric dissolved organic matter ($S_{275–295}$) as a tracer of terrigenous dissolved organic carbon in river-influenced ocean margins. Limnol. Oceanogr. 57 (5), 1453–1466.
Follett, C.L., Repeta, D.J., Rothman, D.H., Xu, L., Santinelli, C., 2014. Hidden cycle of dissolved organic carbon in the deep ocean. P. Natl. Acad. Sci. USA. 111 (47), 16706–16711.
Gearing, J.N., 1998. The use of stable isotope ratios of tracing the nearshore-offshore exchange of organic matter. In: Jansson, B.-O. (Ed.), Coastal-Offshore Ecosystem Interactions. Springer, Berlin, Heidelberg, pp. 69–101.
Gong, G.-C., Wen, Y.-H., Wang, B.-W., Liu, G.-J., 2003. Seasonal variation of chlorophyll a concentration, primary production and environmental conditions in the subtropical East China Sea. Deep-sea Res. Pt II 50 (6–7), 1219–1236.
Gu, H., Moore, W.S., Zhang, L., Du, J., Zhang, J., 2012. Using radium isotopes to estimate the residence time and the contribution of submarine groundwater discharge (SGD) in the Changjiang effluent plume, East China Sea. Cont. Shelf Res. 35, 95–107.
Guo, L., Macdonald, R.W., 2006. Source and transport of terrigenous organic matter in the upper Yukon River: evidence from isotope ($\delta^{13}C$, $\Delta^{14}C$, and $\delta^{15}N$) composition of dissolved, colloidal, and particulate phases. Glob. Biogeochem. Cy. 20 (2), GB2011.
Hansell, D.A., 2005. Dissolved organic carbon reference material program. EOS Trans. Am. Geophys. Union 86 (35), 318.
Hedges, J.I., Kiel, R.G., 1995. Sedimentary organic matter preservation: an assessment and speculative synthesis. Mar. Chem. 49, 81–115.
Hedges, J.I., Ertel, J.R., Quay, P.D., Grootes, P.M., Richey, J.E., Devol, A.H., Farwell, G. W., Schmidt, F.W., Salati, E., 1986. Organic carbon-14 in the Amazon River system. Science 231 (4742), 1129–1131.
Hopkinson, C.S., Vallino, J.J., 2005. Efficient export of carbon to the deep ocean through dissolved organic matter. Nature 433, 142–145.
Huang, T.-H., Fu, Y.-H., Pan, P.-Y., Chen, C.-T.A., 2012. Fluvial carbon fluxes in tropical rivers. Curr. Opin. Environ. Sustain. 4 (2), 162–169.
Hung, J.-J., Chen, C.-H., Gong, G.-C., Sheu, D.-D., Shiah, F.-K., 2003. Distributions, stoichiometric patterns and cross-shelf exports of dissolved organic matter in the East China Sea. Deep-sea Res. Pt II 50, 1127–1145.
Hur, H.B., Jacobs, G.A., Teague, W.J., 1999. Monthly variations of water masses in the yellow and East China seas, November 6, 1998. J. Oceanogr. 55, 171–184.
Ichikawa, H., Beardsley, R.C., 2002. The current system in the yellow and East China seas. J. Oceanogr. 58, 77–92.
Kanakidou, M., Duce, R.A., Prospero, J.M., Baker, A.R., Benitez-Nelson, C., Dentener, F. J., Hunter, K.A., Liss, P.S., Mahowald, N., Okin, G.S., Sarin, M., Tsigaridis, K., Uematsu, M., Zamora, L.M., Zhu, T., 2012. Atmospheric fluxes of organic N and P to the global ocean. Glob. Biogeochem. Cy. 26, GB3026.
Kawakami, H., Kusakabe, M., 2008. Surface water mixing estimated from ^{228}Ra and ^{226}Ra in the northwestern North Pacific. J. Environ. Radioact. 99 (8), 1335–1340.
Kim, T.-H., Kim, G., 2010. Distribution of dissolved organic carbon (DOC) in the southwestern East Sea in summer. Ocean Pol. Res. 32 (3), 291–297.
Kim, J., Kim, G., 2015. Significant anaerobic production of fluorescent dissolved organic matter in the deep East Sea (sea of Japan). Geophys. Res. Lett. 43 (14), 7609–7616.
Kim, G., Lee, K.-K., Park, K.-S., Hwang, D.-W., Yang, H.-S., 2003. Large submarine groundwater discharge (SGD) from a volcanic island. Geophys. Res. Lett. 30 (21), 2098.
Kim, G., Ryu, J.-W., Yang, H.-S., Yun, S.-T., 2005. Submarine groundwater discharge (SGD) into the Yellow Sea revealed by ^{228}Ra and ^{226}Ra isotopes: implications for global silicate fluxes. Earth Planet. Sci. Lett. 237 (1–2), 156–166.
Kim, T.-H., Kwon, E., Kim, I., Lee, S.-A., Kim, G., 2013. Dissolved organic matter in the subterranean estuary of a volcanic island, Jeju: importance of dissolved organic nitrogen fluxes to the ocean. J. Sea Res. 78, 18–24.
Kim, J., Cho, H.-M., Kim, G., 2015. ^{228}Ra flux in the northwestern Pacific marginal seas: implications for disproportionally large submarine groundwater discharge. Ocean Sci. J. 50 (2), 195–202.
Kim, J., Cho, H.-M., Kim, G., 2018. Significant production of humic fluorescent dissolved organic matter in the continental shelf waters of the northwestern Pacific Ocean. Sci. Rep. 8, 4887.
Kim, J., Kim, T.-H., Park, S.R., Lee, H.J., Kim, J.K., 2020. Factors controlling the distributions of dissolved organic matter in the East China Sea during summer. Sci. Rep. 10, 11854.
Kowalczuk, P., Copper, W.J., Whitehead, R.F., Durako, M.J., Sheldon, W., 2003. Characterization of CDOM in an organic rich river and surrounding coastal ocean in the South Atlantic bight. Aquat. Sci. 65 (4), 381–398.
Kowalczuk, P., Zablocka, M., Sagan, S., Kulinski, K., 2010. Fluorescence measured in situ as a proxy of CDOM absorption and DOC concentration in the Baltic Sea. Oceanologia 52 (3), 431–471.
Kuhlbusch, T., 1998. Black carbon and the carbon cycle. Science 280 (5371), 1903.
Lang, S.Q., Lilley, M.D., Hedge, J.L., 2007. A method to measure the isotopic (^{13}C) composition of dissolved organic carbon using a high temperature combustion instrument. Mar. Chem. 103, 318–326.
Lawaetz, A.J., Stedmon, C.A., 2009. Fluorescence intensity calibration using the raman scatter peak of water. Appl. Spectrosc. 63 (8), 936–940.
Lee, S.-A., Kim, G., 2018. Sources, fluxes, and behaviors of fluorescent dissolved organic matter (FDOM) in an estuarine mixing zone: results from the Nakdong-River estuary. Biogeosciences 15, 1115–1122.
Lee, H., Kim, G., Kim, J., Park, G., Song, K.-H., 2014. Tracing the flow rate and mixing ratio of the Changjiang diluted water in the northwestern Pacific marginal seas using radium isotopes. Geophys. Res. Lett. 41, 4637–4645.
Li, X., Wang, W., Chu, P.C., Zhao, D., 2015. Low-frequency variability of the Yellow Sea cold water mass identified from the China coastal waters and adjacent seas reanalysis. Adv. Meteorol. 269859.
Lie, H.-J., Cho, C.-H., 2016. Seasonal circulation patterns of the yellow and East China Sea derived from satellite-tracked drifter trajectories and hydrographic observations. Prog. Oceanogr. 146, 121–141.
Liu, L., Gao, L., 2019. Dynamics of dissolved and particulate organic matter in the Changjiang (Yangtze River) estuary and the adjacent East China Sea shelf. J. Mar. Syst. 198, 103188.
Maher, D.T., Eyre, B.D., 2010. Benthic fluxes of dissolved organic carbon in three temperate Australian estuaries: implications for global estimates of benthic DOC fluxes. J. Geophys. Res. 115, G04039.
Mannino, A., Signorini, S.R., Novak, M.G., Wilkin, J., Friedrichs, M.A.A., Najjar, R.G., 2016. Dissolved organic carbon fluxes in the middle Atlantic bight: an integrated approach based on satellite data and ocean model product. J. Geophys. Res. Biogeosci. 121, 312–336.
Masiello, C.A., Druffel, E.R.M., 1998. Black carbon in deep-sea sediments. Science 280 (5371), 1911–1913.
Maybeck, M., 1982. Carbon, nitrogen, and phosphorus transport by world rivers. Am. J. Sci. 282 (4), 401–450.
Moore, W.S., 1976. Sampling ^{228}Ra in the deep ocean. Deep-Sea Res. Oceanogr. Abstr. 23 (7), 647–651.
Nozaki, Y., Kasemsupaya, V., Tsubota, H., 1989. Mean residence time of the shelf water in the East China and the yellow seas determined by $^{228}Ra/^{226}Ra$ measurements. Geophys. Res. Lett. 16 (11), 1297–1300.
Nozaki, Y., Kasemsupaya, V., Tsubota, H., 1990. The distribution of ^{228}Ra and ^{226}Ra in the surface waters of the northern North Pacific. Geochem. J. 24, 1–6.
Nozaki, Y., Tsubota, H., Kasemsupaya, V., Yashima, M., Ikuta, N., 1991. Residence times of surface water and particle-reactive ^{210}Pb and ^{210}Po in the East China and yellow seas. Geochim. Cosmochim. Ac. 55 (5), 1265–1272.
Painter, S.C., Hartman, S.E., Kivimäe, C., Salt, L.A., Clargo, N.M., Bozec, Y., Daniels, C.J., Jones, S.C., Hemsley, V.S., Munns, L.R., Allen, S.R., 2016. Carbon exchange between a shelf sea and the ocean: the Hebrides shelf, west of Scotland. J. Geophys. Res. Oceans 121, 4522–4544.
Painter, S.C., Lapworth, D.J., Malcolm, E., Woodward, S., Kroeger, S., Evans, C.D., Mayor, D.J., Sanders, R.J., 2018. Terrestrial dissolved organic matter distribution in the North Sea. Sci. Total Environ. 630, 630–647.
Panetta, R.J., Ibrahim, M., Gélinas, Y., 2008. Coupling a high-temperature catalytic oxidation total organic carbon analyzer to an isotope ratio mass spectrometer to measure natural-abundance $\delta^{13}C$-dissolved organic carbon in marine and freshwater samples. Anal. Chem. 80 (13), 5232–5239.
Raymond, P.A., Bauer, J.E., 2001a. Riverine export of aged terrestrial organic matter to the North Atlantic Ocean. Nature 409, 497–500.
Raymond, P.A., Bauer, J.E., 2001b. Use of ^{14}C and ^{13}C natural abundances for evaluating riverine, estuarine, and coastal DOC and POC sources and cycling: a review and synthesis. Org. Geochem. 32 (4), 469–485.
Shi, G., Peng, C., Wang, M., Shi, S., Yang, Y., Chu, J., Zhang, J., Lin, G., Shen, Y., Zhu, Q., 2016. The spatial and temporal distribution of dissolved organic carbon exported from three Chinese rivers to the China Sea. PLoS One 11 (10), e0165039.
Stedmon, C.A., Bro, R., 2008. Characterizing dissolved organic matter fluorescence with parallel factory analysis: a tutorial. Limnol. Oceanogr. Methods 6 (11), 572–579.
Troyer, I.D., Bouillon, S., Barker, S., Perry, C., Coorevits, K., Merckx, R., 2010. Stable isotope analysis of dissolved organic carbon in soil solutions using a catalytic combustion total organic carbon analyzer-isotope ratio mass spectrometer with a cryofocusing interface. Rapid Commun. Mass Sp. 24 (3), 365–374.
Tsunogai, S., Watanabe, S., Sato, T., 1999. Is there a "continental shelf pump" for the absorption of atmospheric CO_2? Tellus 51B (3), 701–712.
Walker, B.D., Guilderson, T.P., Okimura, K.M., Peacock, M.B., McCarthy, M.D., 2014. Radiocarbon signatures and size-age-composition relationships of major organic matter pools within a unique California upwelling system. Geochim. Cosmochim. Acta 126, 1–17.
Wang, S.-L., Chen, C.-T.A., Hong, G.-H., Chung, C.-S., 2000. Carbon dioxide and related parameters in the East China Sea. Cont. Shelf Res. 20 (4–5), 525–544.
Wang, X., Ma, H., Li, R., Song, Z., Wu, J., 2012. Seasonal fluxes and source variation of organic carbon transported by two major Chinese Rivers: the Yellow River and Changjiang (Yangtze) river. Glob. Biogeochem. Cy. 26 (2), GB2025.
Willey, J.D., Kieber, M.S., Eyman, M.S., Avery, G.B., 2000. Rainwater dissolved organic carbon: concentrations and global flux. Glob. Biogeochem. Cy. 14 (1), 139–148.

Williams, P.M., Druffel, E.R.M., 1987. Radiocarbon in dissolved organic matter in the central North Pacific Ocean. Nature 330, 246–248.
Yan, G., Kim, G., 2012. Dissolved organic carbon in the precipitation of Seoul, Korea: implications for global wet depositional flux of fossil-fuel derived organic carbon. Atmos. Environ. 59, 117–124.
Yunshan, Q., Fan, L., Shanmin, X., 1988. Study on suspended matter in seawater in the southern Yellow Sea. Chin. J. Oceanol. Limnol. 6, 201–215.